Article

Integrable Near-Infrared Photodetectors Based on Hybrid Erbium/Silicon Junctions

Mariano Gioffre' [1], Giuseppe Coppola[1] , Mario Iodice[1] and Maurizio Casalino[1,*]

[1] Institute for Microelectronics and Microsystems, National Research Council, I-80131, Napoli, Italy; mariano.gioffre@cnr.it; giuseppe.coppola@cnr.it; mariano.iodice@cnr.it; maurizio.casalino@cnr.it

* Correspondence: maurizio.casalino@na.immcnr.it; Tel.: +39-81-6132345

Abstract: This paper presents the design, fabrication and characterization of Schottky erbium/silicon photodetectors working at 1.55 μm. These erbium/silicon junctions are carefully characterized using both electric and optical measurements at room temperature. A Schottky barrier Φ_B of ~673 meV is extrapolated; the photodetectors show external responsivity of 0.55 mA/W at room temperature under a 8 V of reverse bias applied. In addition, the device performance is discussed in terms of normalized noise and noise equivalent power. To the best of our knowledge, these are the first Er/Si photodetectors designed for operation in free space at 1.55 μm. The proposed devices will pave the way towards development of Er-based photodetectors and light sources to be monolithically integrated in the same silicon substrate and both operating at 1.55 μm.

Keywords: silicon; near-infrared; photodetectors, internal photoemission; erbium.

1. Introduction

The integrated photonics refers to the fabrication and integration of several photonic components on the same planar substrate. These components include beam splitters, gratings, couplers, polarizers, interferometers, sources and detectors, among others. In the last three decades, there has been growing interest in the use of silicon (Si) as substrate for integrated photonics [1]. In this context, tremendous progresses in the technological processes based on the use of silicon-on-insulator (SOI) substrates have allowed to obtain reliable and effectiveness optical components fully compatible with the complementary metal-oxide semiconductor (CMOS) technology, such as: low loss waveguides, high-Q resonators, high speed modulators and couplers, typically operating at near-infrared wavelengths [2-7].

However, the silicon indirect band-gap and the minimal optical absorption at NIR wavelengths limit the use of Si for some active optical components like sources (led, laser) or NIR photodetectors (PDs).

The latter issue is typically addressed by the integration with Germanium (Ge). Unfortunately, the growth of Ge on a Si substrate is only achievable with a two-step epitaxial growth technique [8, 9] that causes problems in both thermal budget and planarity [10] hindering the monolithically integration of an electronic and photonic circuitry on the same Si substrate. Indeed, Intel [11] and Luxtera [12] reported on four-channel optical receiver working at 50 Gbps and 40 Gbps, respectively, based on Ge PDs that are separately fabricated and only subsequently flip-chip mounted to a Si electronic circuitry. In addition, there has been progress in fabricating SiGe-based PDs in such a 'zero-change' CMOS process flow [13], but the Ge content of the available layer is estimated to be 25% to 35% [14] and consequently the wavelength of possible detection is limited to less than 1200 nm [15]. A single-chip microprocessor integrating over 70 million transistors and 850 photonic components has been fabricated taking advantage of SiGe PDs fabricated by a 'zero-change' CMOS approach operating at 1180 nm [16]. Unfortunately, no Ge-based PDs operating at 1550 nm has been realized by a 'zero change' approach as far.

Thanks to the success of the so-called EDFA (Erbium-doped fiber amplifier) used in telecommunications, in the last years many efforts have been aimed to introduce Er in Si in order to realize Si-based light sources. Unfortunately Si is not a good host for Er. The reason is believed to be linked to a back-transfer process of energy that strongly reduces the light emission at room temperature. The attractive features of this technology are the emission in the telecommunications band of 1550 nm as well as the electrical pumping. For this aim, metal-oxide-semiconductor (MOS) structures are typically realized: a voltage applied between metal and Si causes electrons to tunnel through the oxide in which Er ions are dispersed, exciting them. In a subsequent version of the device Si nanocrystals are dispersed together Er ions in the oxide. Light emitting diodes based on this approach show efficiencies of about 10% as reported by STMicroelectronics [17] even if the light emission is observed to diminish when the current density increases. This effect is believed to be due to free carrier absorption and Auger processes, thus, despite of first preliminary successes, many concerns need still to be addressed

Although Erbium results a very promising material for the realization of Si-based LASER, no investigations have been performed on the use of hybrid Er/Si structures in the field of the near-infrared detection. Indeed, this could be very fascinating in the vision of integrating both Er-based LASER and PDs on the same silicon substrate. In addition, Er can be deposited by sputtering at low temperature without compromising an eventually pre-existent electronic circuitry. On the other hand, sputtered Er deposited on Si has already shown the capability to form Schottky junctions [18] that have been widely employed in both infrared and NIR detection [19-23].

In this work we report on Er-based Schottky PDs operating at 1550nm and integrated with a double-polished 200μm-thick Si substrate. Er has been deposited by a radio-frequency (RF) sputtering process at low temperature and its optical properties have carefully been characterized by ellipsometric techniques. The photocurrent generation is based on the internal photoemission effect, where photoexcited carriers from Er are emitted into Si over the Schottky barrier Φ_{B0}. The rectifying Schottky diode behavior is shown from the IV curve, from which both the series resistance and the ideality coefficients are extrapolated together with a Schottky barrier Φ_{B0} of ~673 meV. We show that an external responsivity (photogenerated current-incident optical power ratio) of R_{ext}~0.29 mA/W at 1V reverse bias, can be obtained; this value increases up to ~0.55 mA/W when a reverse voltage of 8V is applied. We believe that this work paves the way to the realization of microsystems where Er-based sources and photodetectors are monolithically integrated on the same Si substrate.

2. Materials and Methods

2.1 Erbium deposition

A Radio-Frequency (RF) Sputtering technique was used for depositing the Erbium (Er) thin film directly on the Si substrate, from a 99,9% pure metal Er target. The substrate was placed on the holder and the deposition chamber was pumped down to a base pressure of $3 \cdot 10^{-6}$ mbar before introducing the process gas (Ar). Er film was then deposited at r.t., with 30 W RF power, at $2.5 \cdot 10^{-2}$ mbar pressure, with a constant 40 sccm Ar flux and 11 min deposition time. To overcome the target surface oxidation a 30 min presputtering process at 150 W RF power was necessary before the deposition process.

2.2 Erbium ellipsometric characterization

Spectroscopic ellipsometry data were recorded using a phase modulated spectroscopic ellipsometer (UVSEL, Jobin Yvon Horiba) with a wavelength scanning range from 300 to 1600 nm, at an incident angle of 70°. Acquired data were fit to an optical model of the sample in which the dispersion of the erbium film was assumed to follow a classical dispersion model [24, 25] based on the sum of the single and double Lorentz, and Drude oscillators:

$$\tilde{\varepsilon}(\omega) = \varepsilon_\infty + \frac{(\varepsilon_s - \varepsilon_\infty)\cdot\omega_t^2}{\omega_t^2 - \omega^2 + j\Gamma_0\cdot\omega} + \frac{\omega_p^2}{-\omega^2 + j\Gamma_d\cdot\omega} + \sum_{i=1}^{2} \frac{f_i\cdot\omega_{0i}^2}{\omega_{0i}^2 - \omega^2 + j\cdot\gamma_i\cdot\omega} \quad (1)$$

The Lorentz oscillator model works well for insulators and semiconductors above the band gap, while the Drude model describes well the optical properties of metals but does not take into account the notion of optical band gap energy Eg. The combination of both is often adequate when the material is a little conductive and has a metallic character. In our case, for the erbium dielectric function assessment, was introduced only one of the two oscillators of the last term. Fitting of experimental data leads to film thickness and dielectric function $\tilde{\varepsilon} = \varepsilon_1 - j\varepsilon_2$ evaluation; the complex refractive index come from the dielectric function assuming that $\tilde{\varepsilon} = n^2 = (n - jk)^2$. The film structure used in the model consists of a homogeneous bulk erbium film and an outmost layer, described by a Bruggeman effective medium approximation (BEMA) [26].

2.3 Electrical characterizatione

To electrically characterize the PD, we measure the current-voltage (I-V) characteristics of the Er/p-Si Schottky junction when p-Si is biased with respect to grounded Er electrode. The I-V characteristics were acquired using a Keithley 6487 picoammeter. Fig. 3a is the mean of five curves that were obtained by varying the voltages repetitively from −8 V to 2 V and vice-versa.

2.3 Optoelectronic characterization

For optoelectronic characterization, a tunable NIR laser (AQ4321D, Ando) was collimated, chopped and split into two beams using a beam splitter. One beam was focused by a 20× IR microscope objective (MO) to the device under test (DUT). The transmitted light was collected using a 20× IR collecting MO and addressed on a NIR CCD to simplify the alignment procedure. A lock-in amplifier was used to measure the photocurrent produced by the DUT. The second beam was sent to a calibrated commercial power meter to perform incident optical power measurements and, consequently, to calculate the external responsivity.

3. Results and discussion

3.1. Fabrication and theoretical background

Devices reported in Figure 1 have been fabricated starting from a bi-polished 200-μm-thick very lightly doped P silicon. Substrate was chosen slightly doped in order to avoid free carrier absorption.

After a RCA Si cleaning process, the Si substrate has been thermally oxidized in order to obtain a 100-nm-thick silicon dioxide (SiO_2). The two electrodes, the collecting Ohmic contact and the Schottky contact, were both realized on the top of the substrate. The collecting contact was made by a ring of 200-nm-thick aluminium film, thermally evaporated at $3x10^{-6}$ mbar and 150 °C.

First of all the Shipley S1813 photoresist (PR) was deposited by spin coating at 4000 rpm, by resulting in a PR thickness of 1.4 μm and then a standard photolithography process was used to form a ring pattern. After that a SiO_2 wet etching process was performed and, after the aluminium thermal evaporation, a lift-off process was carried out in order to obtain a directly contact between Al and Si. Then an annealing at 475 °C in nitrogen for 30 min, to get a not-rectifying behaviour, was carried out.

The Schottky contact was fabricated by sputtering deposition of 50 nm thick erbium film. The top of the wafer was covered by Shipley S1813 PR, exposed and developed in order to obtain a disk surrounded by the Al ring Ohmic contact.

Preprints (www.preprints.org) | NOT PEER-REVIEWED | Posted: 28 September 2018 doi:10.20944/preprints201809.0572.v1

Peer-reviewed version available at Sensors 2018, 18, 3755; doi:10.3390/s18113755

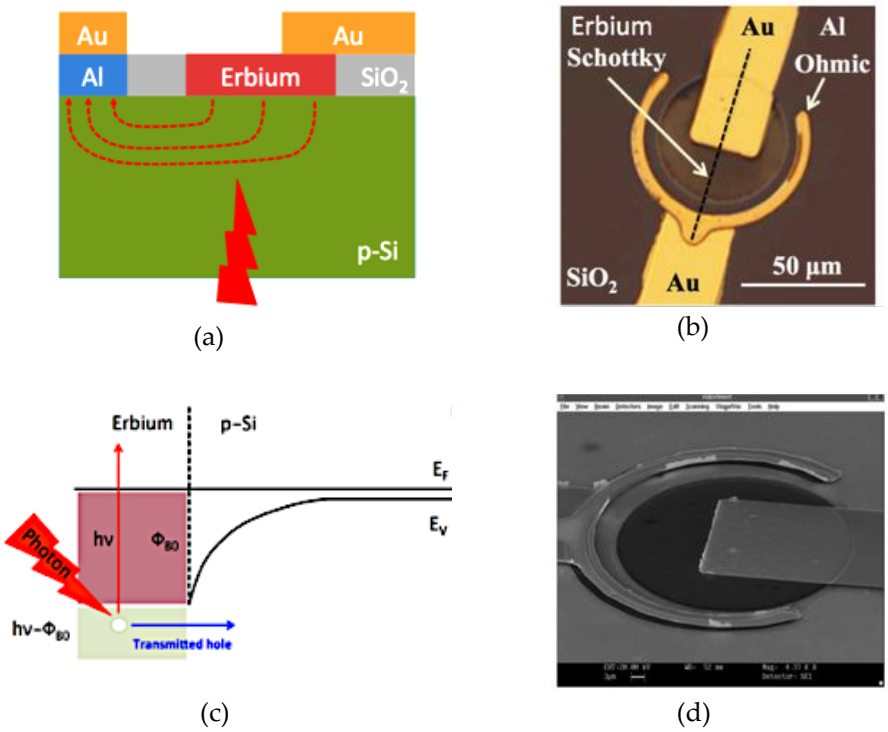

Figure 1. (a) Schematic cross-sectional view of the graphene/Si Schottky PD under illumination; **(b)** optical image of a sample device; **(c)** the IPE mechanism in a Er/p-Si Schottky junction, where E_F is the Fermi energy of the metal, E_V is the Si valence band energy and hv-Φ_B is the differerence between the photon energy and the Schottky barrier; **(d)** SEM image of the device.

Then the Ebium active materials was deposited as reported in the Section 2 and subsequently patterned. Finally, two gold (Au) electrodes have been realized, by standard pholitography and lift-off process, in order to connect both Schottky (Er) and Ohmic (Al) contact of the device to the macroscopic world.

Internal quantum efficiency of Si-based Schottky PDs can be written as $\eta_{int} = C \cdot \frac{(hv-\Phi_B)^2}{hv}$ [27, 28], where C is the quantum efficiency coefficient, hv is the energy photon and Φ_B is the Schottky barrier height (SBH). On the other hand, η_{int} is linked to the external responsivity $\eta_{ext} = A \cdot \eta_{int}$, where A is the metal absorption can be written as:

$$A = (1 - R) \cdot (1 - e^{-\alpha \cdot d}) \quad (2)$$

where R is the reflectivity at the metal/Si interface, α and d are the absorption coefficient and thickness of the metal, respectively. The absorption coefficient α is linked to the penetration depth $\delta=1/\alpha$, thus in the limit of metal thickness $d>>\delta$, all optical power going in the metal will be absorbed and A=1-R. This means that the lower the reflectivity the higher the absorption (and the higher the efficiency). The corresponding external responsivity can be written as [26]:

$$R_{ext} = \frac{q}{hv} \cdot \eta_{ext} = (1 - R) \cdot C \cdot \frac{(hv-\Phi_B)^2}{hv^2} \left[\frac{A}{W}\right] \quad (3)$$

3.2. Erbium Charactherization

Figure 2 shows the ellipsometric characterization carried out on the sputtered Er in term of complex refractive index and reflectivity.

Preprints (www.preprints.org) | NOT PEER-REVIEWED | Posted: 28 September 2018 doi:10.20944/preprints201809.0572.v1

Peer-reviewed version available at Sensors 2018, 18, 3755; doi:10.3390/s18113755

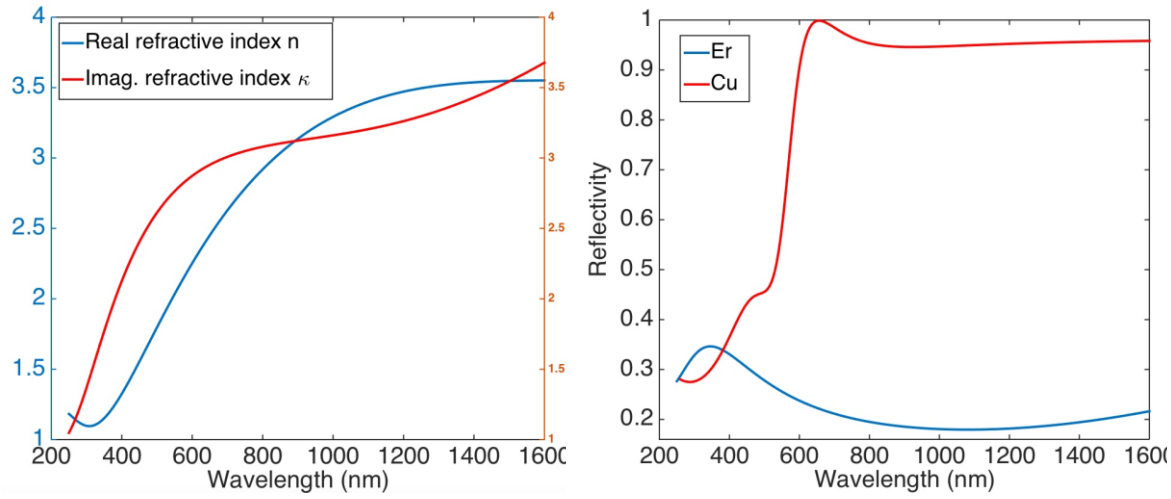

(a) (b)

Figure 2. (**a**) real (blue) and imaginary (red) refractive index of sputtered Er measured by ellipsometric characterization; **(b)** Simulated reflectivity at both Si/Cu and Si/Er interface for normal incidence.

Figure 2(a) shows that Er is characterized by a extinction coefficient of κ=3.68 at λ_0=1550 nm; it leads to an absorption coefficient ($\alpha=4\pi\kappa/\lambda_0$) and penetration depth ($\delta=1/\alpha$) of 29.8 μm^{-1} and 33.6 nm at 1550 nm, respectively. By using the Fresnel coefficient for normal incidence the reflectivity of the Si/Er interface is reported in Figure 2(b) where the reflectivity of Si/Cu interface is reported for comparison, too.

3.3. Electrical charactherization

Fig. 3(a) shows the I-V experimental characteristics of the Er/p-Si Schottky junction.

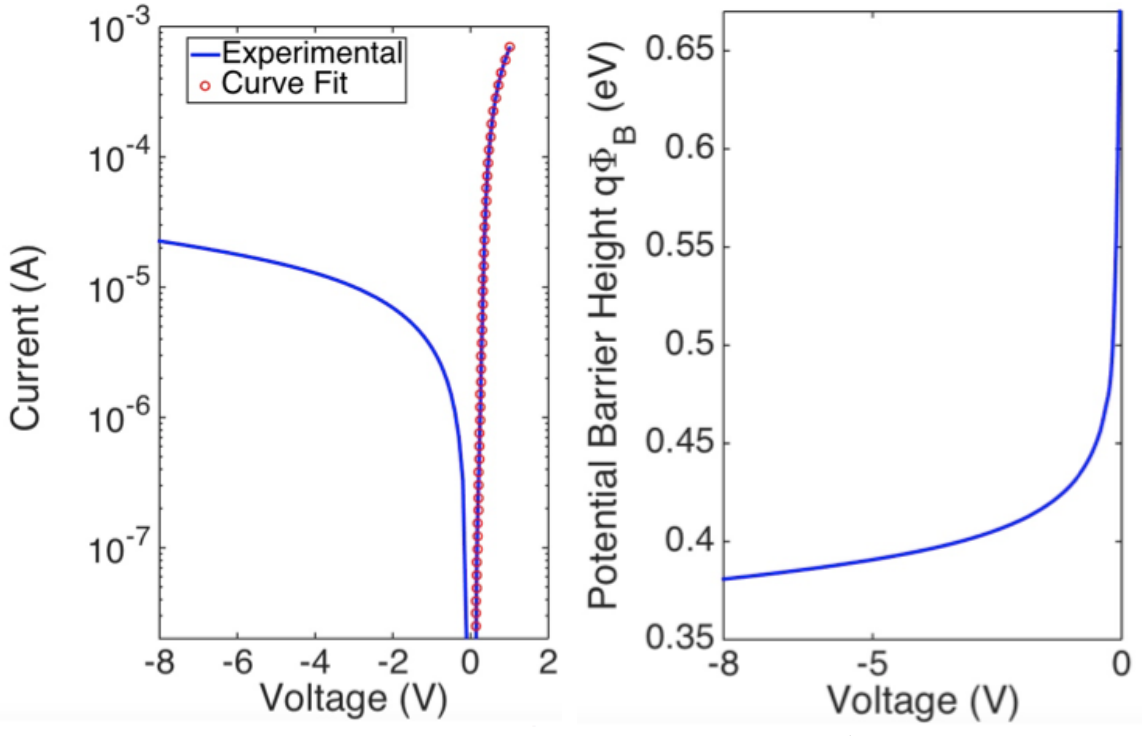

(a) (b)

Figure 3. (a) *I-V* characteristics of Er/p-Si PD at room temperature; **(b)** Potential barrier height as a function of reverse bias.

Preprints (www.preprints.org) | NOT PEER-REVIEWED | Posted: 28 September 2018 doi:10.20944/preprints201809.0572.v1

Peer-reviewed version available at Sensors 2018, 18, 3755; doi:10.3390/s18113755

The device shows rectifying I–V diode behavior, which follows the Schottky diode equation [29]:

$$I = I_S \cdot \left(e^{\frac{q(V - R_S I)}{\eta k_B T}} - 1 \right) \quad (4)$$

$$I_S = AA^* T^2 e^{-\frac{q\Phi_B}{k_B T}} \quad (5)$$

where $\Phi_B(V) = \Phi_{B0} - \Delta\Phi(V)$, Φ_{B0} is the SBH at zero voltage, $\Delta\Phi_B(V)$ is the SBH change due to applied voltage, A* is the Richardson constant (32 A/cm² K² for p-type Si [30]), A is the junction area, k_BT~26 meV at room temperature, η is the diode ideality factor, defined as the deviation of the measured I–V curve from the ideal exponential behaviour [30], and V is the external applied voltage. In the low injection regime (V<0.51V), the device shows negligible series resistance as highlighted from the linear behaviour shown in Fig. 3(a), however at higher voltages the current deviates from the linearity and R_s cannot be neglected anymore. $\Delta\Phi_B(V)$ is significant in reverse bias where a barrier-lowering Schottky due to image force effect occurs [30] but it can be neglected in forward bias where $\Phi_B \sim \Phi_{B0}$ can be assumed. We estimate SBH in forward bias by fitting the experimental data with Eqs. (3) and (4) and by using Φ_B, η and R_s as fitting parameters. We get Φ_B=0.673±0.003 eV, η=1.16±0.01 and R_s=823±3 Ω. An ideality factor η close to the unity indicates that the Er/p-Si junction has a behaviour that can be well approximated by the canonical equation of the Schottky junctions.

Φ_{B0} can also be estimated by the experimental reverse current shown in Figure 3(a) and by reverting Eq. (5) in order to plot $\Phi_B(V)$. In the limit V→0 this confirms a value of Φ_{B0}~0.67 eV. Finally Figure 3(b) shows the SBH dependence on applied reverse voltage and find $\Delta\Phi_B$ up to ~0.29 eV at V=-8V.

3.4. Electro-Optical characterization

The optoelectronic characterizations are carried out using the setup of Figure 4 (a) and described in Section 2. Figure 4 (b) plots the spectral response under reverse voltage V=-1V.

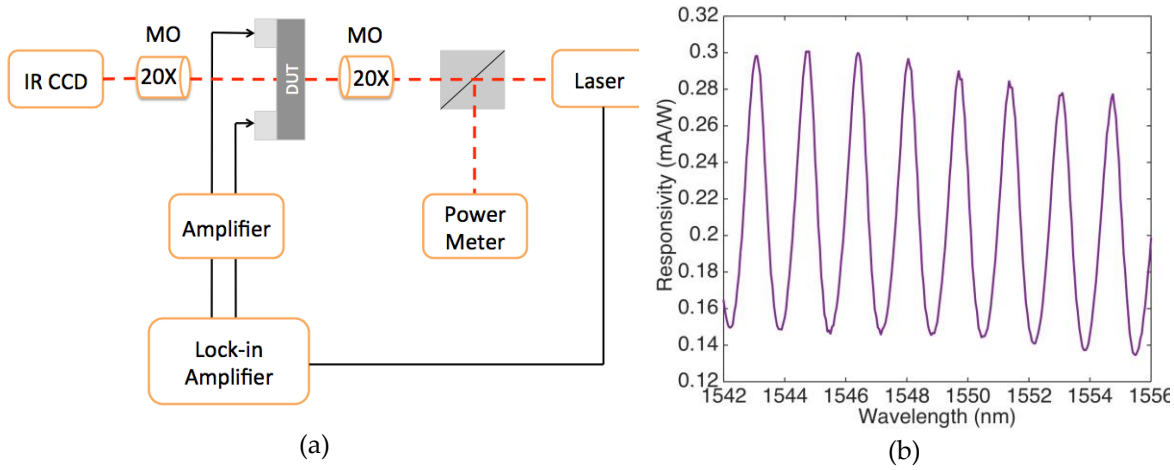

(a) (b)

Figure 4. (a) Optoelectronic measurements setup. (b) Spectral external responsivity Re/Si Schottky PD at V = -1 V.

Device shows many resonance fringes. They are due to the 200um-thick silicon layer behaves as a low finesse Fabry-Perot microcavity, thus when the wavelength is in agreement with the cavity length the optical field is enhanced in the Si cavity leading to an increased Er absorption. The spectral separation between the peaks is ~1.7 nm, matching that one of the Fabry–Perot cavity that is $FSR=\lambda^2/2n_{Si}L$=1.65 nm, being λ the wavelength, and n_{Si} and L the Si refractive index and cavity length, respectively. As expected, at resonance we get photocurrent (responsivity) peaks due to increased absorption at the Er/Si interface. Maximum responsivity is ~0.3 at -1V of reverse bias applied.

Preprints (www.preprints.org) | NOT PEER-REVIEWED | Posted: 28 September 2018 doi:10.20944/preprints201809.0572.v1

Peer-reviewed version available at Sensors 2018, 18, 3755; doi:10.3390/s18113755

To further enhance R_{ext}, we exploit the Schottky barrier lowering effect and apply a larger (up to 8 V) reverse bias to the PDs.

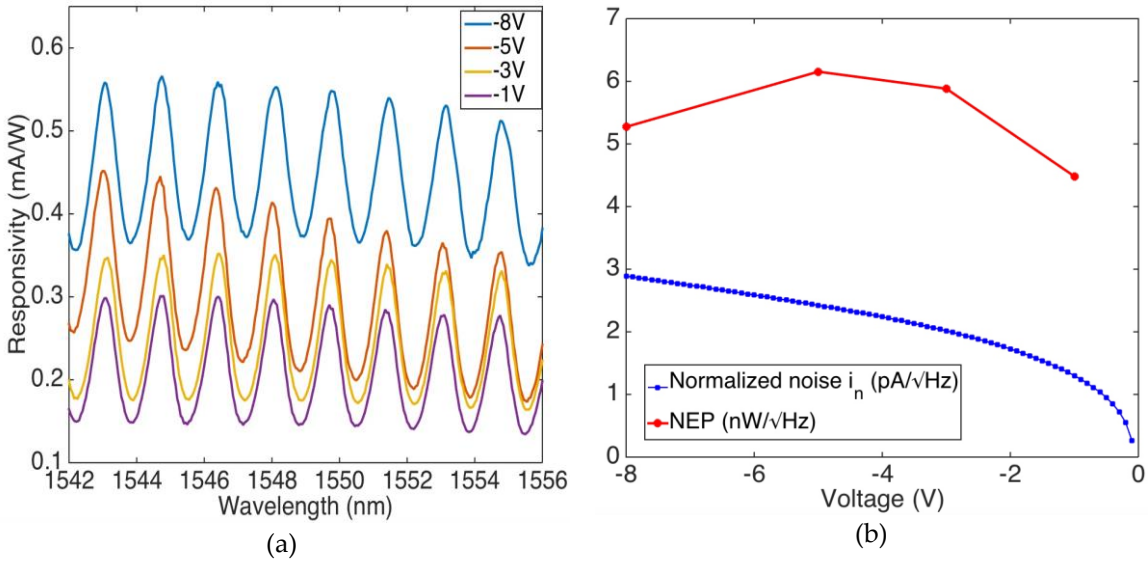

(a) (b)

Figure 5. (**a**) Responsivity vs wavelength at different reverse biases; (**b**) NEP (red circles) and total noise current in (blue squares) at different reverse biases.

Figure 5 (a) plots R_{ext} for different reverse bias. We get R_{ext} ~ 0.55 mA/W at V = -8 V. It could be useful to mentioning that these devices show a responsivity more than two order of magnitude higher than same device realized with copper (Cu) [31]. This remark can be partially explained by considering the Er/Si interface is characterized by a reflectivity one order of magnitude lower than copper as shown in Fig. 2(b) and this lead to increased responsivity as shown in Eq. (3).

To estimate a noise figure of our PD we calculate the noise equivalent power (NEP), i.e., the amount of incident light power that generates a photocurrent equal to the noise current, $NEP = i_n/R_{ext}$ [32]. We assume that Johnson (thermal) and shot (quantum) noise dominating over the low-frequency (1/f) noise [33, 34]. The Johnson (i_j) and shot (i_s) noise currents normalized to the spectral band [1 Hz] are given by $i_j = ((4kT)/R_{eq})^{1/2}$ [29] and $i_s = (2q(I_{ph} + I_d))^{1/2}$ [29], where $R_{eq} = dV/dI$ is the equivalent resistance of a PD at reverse bias in dark, I_{ph} is the photocurrent, I_d is the dark current and $i_n = i_j + i_s$ is the normalized noise. Figure 5 (b) plots both NEP and i_n as a function of the reverse bias applied V and for V =-8 V we get i_n ~ 2.9 pA/Hz$^{0.5}$ and NEP ~ 5.3 nW/Hz$^{0.5}$.

4. Conclusion

In conclusion, we have demonstrated the first free-space Er-based PD for operation at 1.55 μm. The proposed devices are based on Er/pSi Schottky junctions and their photodetection mechanism is based on internal photoemission. The Er/Si junction has been electrically characterized at room temperatures and a series resistance, ideality factor and Schottky barrier of 823 Ω, 1.16 and 673meV have been achieved, respectively. It is worth noting that the ideality factor is close to the unity demonstrating that the Er/pSi junction can be very well described taking advantage of the canonical theory on the Schottky structures.

The PDs are characterized by external responsivity of 0.29 mA/W at 1V; this value increases up to ~0.55 mA/W with a reverse voltage of 8V. Finally, normalized noise and NEP, have been discussed.

The results above indicate the possibility of realization of Si-based free-space PDs that operate at 1.55 μm taking advantage by a rare earth as Er. To the best of our knowledge, this is the first free-space Er/pSi Schottky PD for operation at 1.55 μm. Moreover, it should be noted that the proposed device could be view as a low-finesse Fabry-Perot microcavity where the Er absorption, and so device responsivity, can be periodically increased due to the enhancement of the optical field inside the Si

cavity. In this context, the responsivity may be enhanced through use of an high-finesse Fabry-Pérot optical microcavities, which have previously demonstrated capabilities for provision of greatly increased absorption of the active medium [35]. In addition, the use of a high-finesse Fabry-Pérot optical microcavity would also be beneficial in terms of NEP.

We believe that this work paves the way to the fabrication of Er-based both sources and photodetectors to be monolithically integrated on the same Si substrate.

Re ferences

1. Jalali, B.; Fathpour, S. Silicon Photonics. *J. Lightwave Technol.* **2006**, *24*, 4600-4615, DOI**:** 10.1109/JLT.2006.885782.
2. Rowe, L. K.; Elsey, M.; Tarr, N.G.; Knights, A.P.; Post, E. CMOS-compatible optical rib waveguides defined by local oxidation of silicon. *Electron. Lett.* **2007**,*.43 (7)*, 392-393, DOI: 10.1049/el:20073680.
3. Vivien, L.; Pascal, D.; Lardenois, S.; Marris-Morini, D.; Cassan, E.; Grillot, F.; Laval, S.; Fédéli, J. M.; El Melhaoui, L. Light Injection in SOI Microwaveguides Using High-Efficiency Grating Couplers. *J. Lightwave Technol.* **2006**, *24*, 3810-3815, DOI: 10.1109/JLT.2006.878060.
4. Xu, Q.; Manipatruni, S.; Schmidt, B.; Shakya, J.; Lipson, M. 12.5 Gbit/s carrier-injection-based silicon micro-ring silicon modulators. *Opt. Express* **2007**, *15*, 430-436, DOI: 10.1364/OE.15.000430.
5. Michael, C. P.; Borselli, M.; Johnson, T. J.; Chrystal, C.; Painter, O. An optical fiber-taper probe for wafer-scale microphotonic device characterization. *Opt. Express* **2007**, *15*, 4745-4752 DOI: 10.1364/OE.15.004745.
6. Liu, A.; Liao, L.; Rubin, D.; Nguyen, H.; Ciftcioglu, B.; Chetrit, Y.; Izhaky, N.; Paniccia, M. High-speed optical modulation based on carrier depletion in a silicon waveguide. *Opt. Express* **2007**, *15*, 660-668 DOI: 10.1364/OE.15.000660.
7. Liu, A.; Rong, H.; Jones, R.; Cohen, O.; Hak, D.; Paniccia, M. Optical Amplification and Lasing by Stimulated Raman Scattering in Silicon Waveguides. *J. Lightwave Technol.* **2006**, *24*, 1440-1455 DOI: 10.1109/JLT.2005.863322.
8. Eng, P. C.; Song, S.; Ping, B. State-of-the-art photodetectors for optoelectronic integration at telecommunication wavelength. *Nanophotonics*. **2015**, *4 (3)* 277– 302, DOI: 10.1515/nanoph-2015-0012
9. Michel, J.; Liu, J. L. C. Kimerling, L. C. High-performance Ge-on-Si photodetectors. *Nature Photonics* **2010,** *4*, 527–534, DOI: 10.1038/nphoton.2010.157.
10. Wang, J.; Lee, S. Ge-Photodetectors for Si-Based Optoelectronic Integration. *Sensors* **2011**, *11*, 696-718. DOI: 10.3390/s110100696.
11. Alduino, A. Demonstration of a high speed 4-channel integrated silicon photonics WDM link with hybrid silicon lasers. IEEE Hot Chips 22 Symposium (HCS), Stanford, CA, USA, 22-24 Aug. 2010; IEEE; 1-29, DOI: 10.1109/HOTCHIPS.2010.7480075.
12. Narasimha, A.; Analui, B.; Balmater, E.; Clark, A.; Gal, T.; Guckenberger, D.; Gutierrez, S.; Harrison, M.; Koumans, R.; Kucharski, D.; Liang, Y.; Mekis, A.; Mirsaidi, S.; Peterson, M.; Pham, T.; Pinguet, T.; Sadagopan, V.; Sleboda, T.; Song, D.; Wang, Y.; Welch, B.; Witzens, J.; Abdalla, S.; Gloeckner, S.; De Dobbelaere, P. A 40-Gb/s QSFP Optoelectronic Transceiver in a 0.13µm CMOS Silicon-on-Insulator Technology, Proceedings of Optical Fiber Communication Conference/National Fiber Optic Engineers Conference, San Diego, CA, USA, 24-28 Feb. OSA, paper OMK7.
13. Harame, D.L.; Koester, S. J.; Freeman, G.; Cottrel, P.; Rim, K.; Dehlinger, G.; Ahlgren, D.; Dunn, J. S.; Greenberg, D.; Joseph, A.; Anderson, F.; Rieh, J. S.; Onge, S. A. S. T.; Coolbaugh, D.; Ramachandran, V.; Cressler, J. D.; Subbanna, S. The revolution in SiGe: impact on device electronics. *Appl. Surf. Sci.* **2004**, *224*, 9–17, DOI:10.1016/j.apsusc.2003.08.086.
14. Alloatti, L.; Srinivasan, S. A.; Orcutt, J. S.; Ram, R. J. Waveguide-coupled detector in zero-change complementary metal–oxide–semiconductor. *Appl. Phys. Lett.* **2015**, *107*, 041104, DOI: 10.1063/1.4927393.
15. Meng, H.; Atabaki, A.; Orcutt, J. S.; Ram, R. J. Sub-bandgap polysilicon photodetector in zero-change CMOS process for telecommunication wavelength. *Opt. Express* **2015**, *23*, 32643-32653 DOI: 10.1364/OE.23.032643.
16. Sun,C.; Wade, M.T.; Lee, Y.; Orcutt, J. S.; Alloatti, L.; Georgas, M. S.; Waterman, A. S.; Shainline, J. M.; Avizienis, R. R.; Lin, S.; Moss, B. R.; Kumar, R.; Pavanello, F.; Atabaki, A. H.; Cook, H. M.; Ou, A. J.; Leu, J. C.; Chen, Y.-H.; Asanovic´, K.; Ram, R. J.; Popovic´, M. A.; Stojanovic, V. M. Single-chip microprocessor that communicates directly using light. *Nature* **2015** *528*, 534–538, DOI: 10.1038/nature16454..

17. Castagna, M. E.; Coffa, S.; Carestia, L.; Messian A.; Buongiorno, C. Quantum Dot Materials and Devices for Light Emission in Silicon. Proceedings of 32nd European Solid-State Device Research Conference, Firenze, Italy, 24-26 September 2002; IEEE; 439-442, DOI: 10.1109/ESSDERC.2002.194962.
18. Jang, M; Kim, Y.; Shin, J.; Lee, S. Formation of erbium-silicide as source and drain for decananometer-scale Schottky barrier metal-oxide-semiconductor field-effect transistors. *Materials Science and Engineering B* **2004**, 114-115, 51-55, DOI: 10.1016/j.mseb.2004.07.032.
19. Kimata, M.; Ueno, M.; Yagi, H.; Shiraishi, T.; Kawai, M.; Endo, K.; Kosasayama, Y.; Sone, T.; Ozeki, T.; Tsubouchi, N. PtSi Schottky-barrier infrared focal plane arrays, *Opto-Electron. Rev.* **1998, 6**, 1–10.
20. Casalino, M; Sirleto, L.; Moretti, L.; Gioffrè, M.; Coppola, G.; Iodice, M.; Rendina, I. Back-Illuminated Silicon Resonant Cavity Enhanced Photodetector at 1550 nm. *Physica E: Low-dimensional Systems and Nanostructures* **2009**, 41, 1097–1101. DOI: 10.1016/j.physe.2008.08.049
21. Berini, P. Surface plasmon photodetectors and their applications. *Laser&Photonics Reviews* **2013**, 8(2), 197-220. DOI: 10.1002/lpor.201300019
22. Casalino, M.; Iodice, M.; Sirleto, L.; Rendina, I.; Coppola, G. Low dark current silicon-on-insulator waveguide metal-semiconductor-metal photodetector based on internal photoemission effect at 1550 nm. *Journal of Applied Physics* **2013**, 114, 153103, DOI: 10.1063/1.4825072
23. Casalino, M.; Russo, R.; Russo, C.; Ciajolo, A.; Di Gennaro, E.; Iodice, M.; Coppola, G. Free-space graphgene/silicon photodetectors aerating at 2 micron. https://arxiv.org/abs/1712.02836.
24. Frederick, W.; *Optical Properties of Solids*; Academic Press, 1972; ISBN: 9781483220765.
25. Hecht, E.; Optics, 4th. Ed.; Addison-Wesley, 2002; ISBN: 0321188780.
26. Bruggeman, D. A. G. Berechnung verschiedener physikalischer Konstanten von heterogenen Substanzen. I. Dielektrizitätskonstanten und Leitfähigkeiten der Mischkörper aus isotropen Substanzen. *Ann. Phys.*, **1935**, 416 (7), 636-664; DOI: 10.1002/andp.19354160705.
27. Christine, S.; Berini, P. Thin-Film Schottky Barrier Photodetector Models. *IEEE J. of Quant. Elect.*, 2010, 46(5), 633, DOI: 10.1109/JQE.2010.2046720
28. Casalino, M. Design of Resonant Cavity Enhanced Schottky Graphene/Silicon Photodetectors at 1550 nm. *Journal of Lightwave Technology*, **2018**, 36(9), 1766-1774. DOI: 10.1109/JLT.2018.2791720
29. Casalino, M. Internal Photoemission: Theory Revisited and Theoretical Limitations on the Performance of Near-Infrared Silicon Schottky Photodetectors . *IEEE J. of Quant. Elect.*, **2016**, 52(4), 4000110. DOI: 10.1109/JQE.2016.2532866
30. Sze, S. M.; Ng, K. K. *Physics of Semiconductor Devices*, 3rd ed.; John Wiley & Sons, New Jersey, 2006; ISBN-I 3: 978-0-47 1-1 4323-9, ISBN-10: 0-471-14323-5
31. Casalino, M.; Sirleto, L.; Moretti, L.; Gioffrè, M.; Coppola, G.; Rendina, I. Silicon resonant cavity enhanced photodetector based on the internal photoemission effect at 1.55 micron: Fabrication and characterization. *Appl. Phys. Lett.*, **2008**, 92, 251104. DOI: 10.1063/1.2952193
32. Silvano D. *Photodetectors. Devices, Circuits and Applications*, Meas. Sci. Technol, Prentice Hall: New Jersey, 2001; Volume 12 , Number 5, ISBN 0-13-020337-8
33. Llopis, O.; Azaizia, S.; Saleh, K.; Ali Slimane, A.; Fernandez, A. Photodiode 1/f noise and other types of less known baseband noises in optical telecommunications devices. Proceeding of Conference: Noise and Fluctuations (ICNF), Montpellier, France, 24-28 June 2013; IEEE; DOI: 10.1109/ICNF.2013.6579014
34. Zhu, M.; Li, X.; Li, X.; Zang, X.; Zhen, Z.; Xie, D.; Fang, Y.; Zhu, H. Schottky diode characteristics and 1/f noise of high sensitivity reduced graphene oxide/Si heterojunction photodetector. *J. Appl. Phys.*, **2016**, *119(12)*, 124303; DOI: 10.1063/1.4944945
35. Casalino, M.; Sassi, U.; Goykhman, I.; Eiden, A.; Lidorikis, E.; Milana, S.; De Fazio, D.; Tomarchio, F.; Iodice, M.; Coppola, G.; Ferrari, A.C. Vertically illuminated, resonant cavity, enhanced graphene-silicon Schottky photodetectors. *ACS Nano*, **2017**, 11, 10955. DOI: 10.1021/acsnano.7b04792